Modelling elastic structures using SPH: comparison between Riemann-based and diffusive term-based stabilization

Coline de Sousa, Guillaume Oger, Damien Violeau, David Le Touzé

Modelling elastic structures using SPH: comparison between Riemann-based and diffusive term-based stabilization

Coline De Sousa
Nantes Université, École Centrale Nantes
CNRS, LHEEA, UMR 6598
F-44000 Nantes, France
coline.de-sousa@ec-nantes.fr

Guillaume Oger
Nantes Université, École Centrale Nantes
CNRS, LHEEA, UMR 6598
F-44000 Nantes, France

Damien Violeau
EDF R&D, École des Ponts / LHSV
Chatou, France

David Le Touzé
Nantes Université, École Centrale Nantes
CNRS, LHEEA, UMR 6598
F-44000 Nantes, France

***Abstract*—In this paper, different SPH formulations for modelling elastic structures are compared. First, diffusive term-based stabilization methods are considered, especially the δ-SPH scheme adapted to this problem. Then, we take interest in schemes stabilized by the introduction of Riemann problem solution in the equations. For hydrodynamic applications, those problems are usually formulated to give solutions in terms of pressure and velocity. As an alternative approach, Parshikov and Medin [1] proposed a linearized Riemann solver for the stress tensor components and the velocity. Since this method is still rarely mentioned in the literature, the present paper aims first at exploring this scheme and presenting its properties. Improvements brought to the initial proposition of Parshikov and Medin are also proposed, in particular the addition of the MUSCL reconstruction scheme to reach the first order accuracy. Finally, this approach is compared with the δ-SPH scheme, revolving around two academic benchmarks.**

I. Introduction

Granular flow study is a major concern for many industrial applications, including scour near offshore construction, avalanches and landslides. These phenomenom involve a porous matrix undergoing large deformations and characterized by a complex behaviour. All these constraints raise the question of the method to adopt to simulate these flows. The ability of SPH to handle large deformations of the medium makes it particularly advantageous for these problems. Various SPH schemes already exist to model the granular medium behaviour, such as the ones developed by Feng *et al.* [2] or Bui and Nguyen [3], both following an elastoplastic approach. For a more accurate but complex model, Ghaïtanellis [4] proposed to use an elasto-viscoplastic approach. However, whatever model is chosen, the question of the stability of the resulting scheme remains.

Different methods to stabilize the SPH scheme have been established. Among them, the most widely used consists of adding diffusive terms in the conservation equations. Following this idea, the artificial viscosity scheme relies on adding a numerical viscous term in the momentum equation, as initiated by Von Neumann et Richtmyer [5] and adapted to SPH by Monaghan [6]. In addition to this term, the δ-SPH scheme developed by Antuono *et al.* [7] and Marrone *et al.* [8] uses another diffusive term in the continuity equation to remove the spurious numerical noise still present in the pressure field when using the artificial viscosity scheme. These diffusive term-based methods have proved to be very efficient, though some local oscillations may be observed in the solution fields. An alternative stabilization technique consists in introducing Riemann problem solution into the equations. This method, far more time-consuming than the previous one, was proposed by Vila [9] in the context of a SPH-ALE formalism and also used by Parshikov and Medin [1].

The schemes presented in the latter article are studied in the present paper. Indeed, most of SPH schemes for modelling structure use a diffusive term-based stabilization. Since Riemann-SPH schemes are rarely mentionned in the litterature for this purpose, this paper proposes here to explore this option. As a matter of simplicity, the problem is here reduced to structures with a linear elastic behaviour. This paper is structured as follows: first, the governing equations for modelling the deformation of an elastic structure are introduced. Then, several stabilization methods are presented and discussed. Eventually, these schemes are validated and compared over the beam vibration benchmark and the wedge impact benchmark.

II. Governing equations

The general equations governing the deformation of a continuous medium are:

$$\frac{D\rho}{Dt} = -\rho(\boldsymbol{\nabla}\cdot\boldsymbol{U}) \quad (1)$$

$$\rho\frac{D\boldsymbol{U}}{Dt} = \boldsymbol{\nabla}\cdot\boldsymbol{\sigma} + \boldsymbol{f} \quad (2)$$

where ρ is the density of the medium, $\boldsymbol{U}$ the velocity field, $\boldsymbol{\sigma}$ the stress tensor field and $\boldsymbol{f}$ is the force density. In structural mechanics, $\boldsymbol{\sigma}$ is traditionally decomposed as:

$$\boldsymbol{\sigma} = -p\boldsymbol{I} + \boldsymbol{S} \quad (3)$$

where p is the pressure, $\boldsymbol{I}$ is the identity matrix and $\boldsymbol{S}$ the deviatoric stress tensor. p can be expressed directly from $\boldsymbol{\sigma}$ through the relation:

$$p = -\tfrac{1}{3}tr(\boldsymbol{\sigma}) \quad (4)$$

Following this decomposition, (2) can be rewritten:

$$\rho\frac{D\boldsymbol{U}}{Dt} = -\boldsymbol{\nabla}p + \boldsymbol{\nabla}\cdot\boldsymbol{S} + \boldsymbol{f} \quad (5)$$

To close the system properly, extra equations must be defined regarding the evolution of stress in the material. In the case of an elastic isotropic material submitted to small deformations, the constitutive equation allowing to determine $\boldsymbol{\sigma}$ is Hooke's law:

$$\mathring{\boldsymbol{\sigma}} = \lambda tr(\dot{\boldsymbol{\epsilon}})\boldsymbol{I} + 2\mathcal{G}\dot{\boldsymbol{\epsilon}} + \dot{\boldsymbol{J}}_{\boldsymbol{\sigma}} \quad (6)$$

where:

- λ and $\mathcal{G}$ are the Lamé coefficients, expressed as:

$$\lambda = \frac{E\nu}{(1+\nu)(1-2\nu)},\ \mathcal{G} = \frac{E}{2(1+\nu)} \quad (7)$$

  where E is Young's modulus and ν is Poisson's ratio
- $\dot{\boldsymbol{A}}$ refers to the material time derivative, defined for all tensor $\boldsymbol{A}$
- $\dot{\boldsymbol{\epsilon}}$ is the strain rate tensor field:

$$\dot{\boldsymbol{\epsilon}} = \tfrac{1}{2}(\boldsymbol{\nabla}\boldsymbol{U} + \boldsymbol{\nabla}\boldsymbol{U}^T) \quad (8)$$

- $\mathring{\boldsymbol{A}}$ refers to the Jaumann temporal derivative, defined for all symmetric tensor $\boldsymbol{A}$:

$$\mathring{\boldsymbol{A}} = \dot{\boldsymbol{A}} + \dot{\boldsymbol{J}}_{\boldsymbol{A}} \quad (9)$$

- $\dot{\boldsymbol{J}}_{\boldsymbol{A}}$ is the Jaumann rate tensor defined by:

$$\dot{\boldsymbol{J}}_{\boldsymbol{A}} = \boldsymbol{A}\dot{\boldsymbol{\omega}} - \dot{\boldsymbol{\omega}}\boldsymbol{A} \quad (10)$$

  with $\dot{\boldsymbol{\omega}}$ the rotation rate tensor:

$$\dot{\boldsymbol{\omega}} = \tfrac{1}{2}(\boldsymbol{\nabla}\boldsymbol{U} - \boldsymbol{\nabla}\boldsymbol{U}^T) \quad (11)$$

If the momentum equation considered is (5) rather than (2), a similar law can be written for $\boldsymbol{S}$:

$$\mathring{\boldsymbol{S}} = 2\mathcal{G}\left(\dot{\boldsymbol{\epsilon}} - \tfrac{1}{3}tr(\dot{\boldsymbol{\epsilon}})\boldsymbol{I}\right) + \dot{\boldsymbol{J}}_{\boldsymbol{S}} \quad (12)$$

Concerning p, since the medium is supposed to be weakly-compressible, we consider the following equation of state:

$$p = c_0^2(\rho - \rho_0) \quad (13)$$

where c_0 and ρ_0 are respectively the speed of sound and the reference density of the material.

III. Stabilisation methods

A. Stabilisation by diffusive terms

The above equations can be discretized in SPH with the use of the traditional gradient and divergence operators. However, as usual an immediate applications of the SPH tools will lead to numerical instabilities. To avoid that, a diffusive-term based stabilization is here applied by considering the δ-SPH scheme.

Firstly written for hydrodynamic applications, the δ-SPH scheme can be adapted for structural mechanics by adding a divergence term for $\boldsymbol{S}$ in the momentum equation. The resulting set of equations is the following:

$$\frac{D\boldsymbol{x}_i}{Dt} = \boldsymbol{U}_i \quad (14)$$

$$\frac{D\rho_i V_i}{Dt} = 0 \quad (15)$$

$$\frac{D\rho_i}{Dt} = -\rho_i \sum_{j\in\Omega_i}(\boldsymbol{U}_j - \boldsymbol{U}_i)\cdot\boldsymbol{\nabla}W_{ij}V_j + \delta h c_0 \sum_{j\in\Omega_i}\boldsymbol{\psi}_{ij}\cdot\boldsymbol{\nabla}W_{ij}V_j \quad (16)$$

$$\frac{D\boldsymbol{U}_i}{Dt} = -\frac{1}{\rho_i}\sum_{j\in\Omega_i}(p_i + p_j)\boldsymbol{\nabla}W_{ij}V_j + \frac{1}{\rho_i}\sum_{j\in\Omega_i}(\boldsymbol{S}_i + \boldsymbol{S}_j)\boldsymbol{\nabla}W_{ij}V_j + \alpha h c_0\frac{\rho_0}{\rho_i}\sum_{j\in\Omega_i}\pi_{ij}\boldsymbol{\nabla}W_{ij}V_j + \boldsymbol{f}_i \quad (17)$$

where:

- $\boldsymbol{x}_i$ and V_i are the position and the volume of the particle i. More generally, all the quantities with index i are linked to the particle i
- W_{ij} is an abbreviation for $W(\boldsymbol{x}_i - \boldsymbol{x}_j)$, where W is the kernel function, taken here as the Wendland second-order polynomial. Ω_i is the set of particles within the support of the kernel applied on the particle i
- α and δ are two parameters to adjust the intensity of both diffusive terms
- h is the smoothing length

- ψ_{ij} is the diffusive term allowing to regulate the pressure field:

$$\boldsymbol{\psi}_{ij} = 2\left(\rho_j - \rho_i\right)\frac{\boldsymbol{x}_j - \boldsymbol{x}_i}{\|\boldsymbol{x}_j - \boldsymbol{x}_i\|^2} - \left(\boldsymbol{\nabla}^R\rho_j + \boldsymbol{\nabla}^R\rho_i\right) \tag{18}$$

with $\boldsymbol{\nabla}^R$ the renormalized gradient defined for any quantity ϕ_i by:

$$\boldsymbol{\nabla}^R\phi_i = \boldsymbol{L}_i\left(\sum_{j\in\Omega_i}(\phi_j - \phi_i)\boldsymbol{\nabla}W_{ij}V_j\right) \tag{19}$$

and $\boldsymbol{L}_i$ the renormalization matrix:

$$\boldsymbol{L}_i = \left(\sum_{j\in\Omega_i}(\boldsymbol{x}_j - \boldsymbol{x}_i)\otimes\boldsymbol{\nabla}W_{ij}V_j\right)^{-1} \tag{20}$$

- π_{ij} is the diffusive term from the artificial viscosity scheme:

$$\pi_{ij} = \frac{(\boldsymbol{U}_j - \boldsymbol{U}_i)\cdot(\boldsymbol{x}_j - \boldsymbol{x}_i)}{\|\boldsymbol{x}_j - \boldsymbol{x}_i\|^2} \tag{21}$$

B. Stabilisation by a Riemann solver

Another solution for treating numerical instabilities is the introduction of a Riemann solver into the scheme. It considers the interaction between two particles i and j as a 1D Riemann problem, on the direction $\boldsymbol{n}_{ij} = \frac{\boldsymbol{x}_i - \boldsymbol{x}_j}{\|\boldsymbol{x}_i - \boldsymbol{x}_j\|}$, where i and j constitute the left and right states, respectively. The goal is then to determine the state at the virtual interface between i and j, located at $x_I = \frac{\boldsymbol{x}_i + \boldsymbol{x}_j}{2}\cdot\boldsymbol{n}_{ij}$ and moving at the velocity $U_I = \frac{\boldsymbol{U}_i + \boldsymbol{U}_j}{2}\cdot\boldsymbol{n}_{ij}$.

1) Considering p and $\boldsymbol{S}$: In their article, Parshikov and Medin [1] established two Riemann solvers. The first one, originally designed for hydrodynamic applications, allows to determine the normal velocity U_{ij}^{*N} and the pressure p_{ij}^* at the interface of the particles i and j:

$$\begin{cases} U_{ij}^{*N} = \frac{(\rho_R c_R \boldsymbol{U}_R + \rho_L c_L \boldsymbol{U}_L)\cdot\boldsymbol{n}_{ij} - p_R + p_L}{\rho_R c_R + \rho_L c_L} & (22) \\ p_{ij}^* = \frac{p_R\rho_L c_L + p_L\rho_R c_R - \rho_R c_R \rho_L c_L(\boldsymbol{U}_R - \boldsymbol{U}_L)\cdot\boldsymbol{n}_{ij}}{\rho_R c_R + \rho_L c_L} & (23) \end{cases}$$

where the indices L and R refer to the left and right states, respectively. Since U_{ij}^{*N} and p_{ij}^* are defined at the virtual interface, we can approximate them by the normal velocity and pressure mean on i and j:

$$U_{ij}^{*N} \longrightarrow \frac{\boldsymbol{U}_i + \boldsymbol{U}_j}{2}\cdot\boldsymbol{n}_{ij} \tag{24}$$

$$p_{ij}^* \longrightarrow \frac{p_i + p_j}{2} \tag{25}$$

Accordingly, the scheme obtained after injection of U_{ij}^{*N} and p_{ij}^* in the equations is decentered, therefore stabilized. In order to use this solver for modelling structures, an extra term for the divergence of $\boldsymbol{S}$ is added to the momentum equation, leading to the following system:

$$\frac{D\boldsymbol{x}_i}{Dt} = \boldsymbol{U}_i \tag{26}$$

$$\frac{D\rho_i V_i}{Dt} = 0 \tag{27}$$

$$\frac{D\rho_i}{Dt} = -\rho_i\sum_{j\in\Omega_i} 2\left(U_{ij}^{*N}\boldsymbol{n}_{ij} - \boldsymbol{U}_i\right)\cdot\boldsymbol{\nabla}W_{ij}V_j \tag{28}$$

$$\frac{D\boldsymbol{U}_i}{Dt} = -\frac{1}{\rho_i}\sum_{j\in\Omega_i} 2\,p_{ij}^*\boldsymbol{\nabla}W_{ij}V_j + \frac{1}{\rho_i}\sum_{j\in\Omega_i}(\boldsymbol{S}_i + \boldsymbol{S}_j)\boldsymbol{\nabla}W_{ij}V_j + \boldsymbol{f}_i \tag{29}$$

Besides these equations, the computation of $\boldsymbol{\nabla}\boldsymbol{U}_i$ required to compute $\dot{\boldsymbol{\epsilon}}_i$ is done with the renormalized antisymmetric gradient operator:

$$\boldsymbol{\nabla}\boldsymbol{U}_i = \sum_{j\in\Omega_i}(\boldsymbol{U}_j - \boldsymbol{U}_i)\otimes\boldsymbol{L}_i\boldsymbol{\nabla}W_{ij}V_j \tag{30}$$

From now on, this scheme will be refered to as the Riemann-p scheme.

2) Considering $\boldsymbol{\sigma}$: The second solver presented in [1] is applicable when the momentum equation of the medium considered is (2). Here, we are interested in the normal velocity and in the components of the stress tensor normal to the particles' virtual interface. To determine these values, we leave the Cartesian coordinate system xyz to consider NST, the coordinate system linked to the virtual interface between i and j: N is the normal vector to the interface plane ($N = \boldsymbol{n}_{ij}$), while S and T are in the latter plane. The transfer matrix from xyz to NST is denoted $\boldsymbol{M}$:

$$\boldsymbol{M} = \begin{cases} \begin{pmatrix} \cos\theta & -\sin\theta \\ \sin\theta & \cos\theta \end{pmatrix} & in\ 2D \\ \begin{pmatrix} \sin\theta\cos\varphi & \cos\theta\cos\varphi & -\sin\varphi \\ \sin\theta\sin\varphi & \cos\theta\sin\varphi & \cos\varphi \\ \cos\theta & -\sin\theta & 0 \end{pmatrix} & in\ 3D \end{cases} \tag{31}$$

where the angles θ and φ are defined on figure 1. Thus, the solver to determine the interface state is:

$$\begin{cases} U_{ij}^{*N} = \frac{\rho_R c_R^l U_R^N + \rho_L c_L^l U_L^N + \sigma_R^{NN} - \sigma_L^{NN}}{\rho_R c_R^l + \rho_L c_L^l} & (32) \\ \sigma_{ij}^{*NN} = \frac{\sigma_R^{NN}\rho_L c_L^l + \sigma_L^{NN}\rho_R c_R^l + \rho_R c_R^l \rho_L c_L^l (U_R^N - U_L^N)}{\rho_R c_R^l + \rho_L c_L^l} & (33) \\ \sigma_{ij}^{*SN} = \frac{\sigma_R^{SN}\rho_L c_L^t + \sigma_L^{SN}\rho_R c_R^t + \rho_R c_R^t \rho_L c_L^t (U_R^S - U_L^S)}{\rho_R c_R^t + \rho_L c_L^t} & (34) \\ \sigma_{ij}^{*TN} = \frac{\sigma_R^{TN}\rho_L c_L^t + \sigma_L^{TN}\rho_R c_R^t + \rho_R c_R^t \rho_L c_L^t (U_R^T - U_L^T)}{\rho_R c_R^t + \rho_L c_L^t} & (35) \end{cases}$$

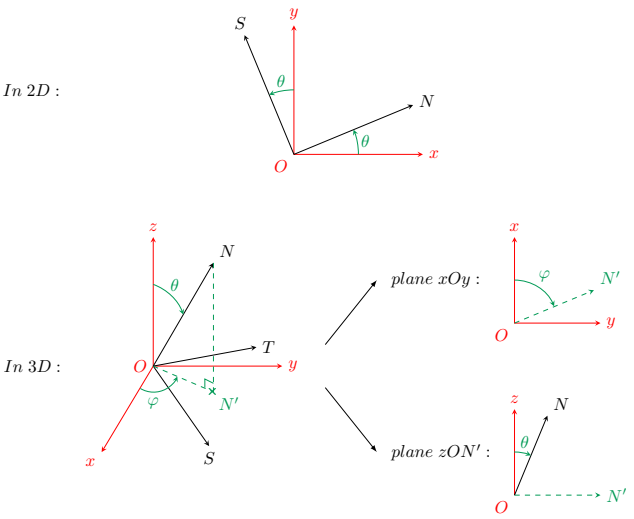

Fig. 1. Change of basis from xyz to NST

where:

- U^N, U^S and U^T are the components of $\boldsymbol{U}$ in NST
- σ^{NN}, σ^{SN} and σ^{TN} are the components of $\boldsymbol{\sigma}\boldsymbol{n}_{ij}$ in NST
- c^l and c^t are the longitudinal wave speed and the transverse wave speed in the material, respectively [11]:

$$c^l = \sqrt{\frac{\lambda + 2\mathcal{G}}{\rho}},\ c^t = \sqrt{\frac{\mathcal{G}}{\rho}} \tag{36}$$

The values obtained for $\boldsymbol{\sigma}$ at the interface are expressed in NST and must be recomputed in xyz, to be introduced later into the equations. As a consequence, we use $\boldsymbol{M}$ to calculate $\boldsymbol{\sigma}_{ij}^{*N}$ in the correct reference frame:

$$\boldsymbol{\sigma}_{ij}^{*N} = \begin{pmatrix} \sigma^{*xN} \\ \sigma^{*yN} \\ \sigma^{*zN} \end{pmatrix}_{ij} = \boldsymbol{M} \begin{pmatrix} \sigma^{*NN} \\ \sigma^{*SN} \\ \sigma^{*TN} \end{pmatrix}_{ij} \tag{37}$$

As before, choices must be done to introduce U_{ij}^{*N} and $\boldsymbol{\sigma}_{ij}^{*N}$ into the equations:

$$U_{ij}^{*N} \longrightarrow \frac{\boldsymbol{U}_i + \boldsymbol{U}_j}{2} \cdot \boldsymbol{n}_{ij} \tag{38}$$

$$\boldsymbol{\sigma}_{ij}^{*N} \longrightarrow \frac{\boldsymbol{\sigma}_i + \boldsymbol{\sigma}_j}{2} \boldsymbol{n}_{ij} \tag{39}$$

By using these relations, we finally obtain the following scheme, later refered to as the Riemann-$\boldsymbol{\sigma}$ scheme:

$$\frac{D\boldsymbol{x}_i}{Dt} = \boldsymbol{U}_i \tag{40}$$

$$\frac{D\rho_i V_i}{Dt} = 0 \tag{41}$$

$$\frac{D\rho_i}{Dt} = -\rho_i \sum_{j\in\Omega_i} 2\,(U_{ij}^{*N}\boldsymbol{n}_{ij} - \boldsymbol{U}_i)\cdot\boldsymbol{\nabla}W_{ij}V_j \tag{42}$$

$$\frac{D\boldsymbol{U}_i}{Dt} = \frac{1}{\rho_i}\sum_{j\in\Omega_i} 2\,\boldsymbol{\sigma}_{ij}^{*N}\|\boldsymbol{\nabla}W_{ij}\|V_j + \boldsymbol{f}_i \tag{43}$$

Moreover, U_{ij}^{*N} needs to be considered in the computation of $\dot{\boldsymbol{\epsilon}}$. Indeed, to ensure the stability of the scheme, the stress tensor must be calculated with U_{ij}^{*N}. In the case of the Riemann-p scheme, (28) links directly U_{ij}^{*N} with $\frac{D\rho}{Dt}$, thus with p through temporal integration and the use of the state equation. Here U_{ij}^{*N} is also directly used to compute $\frac{D\rho}{Dt}$ through (42), but the absence of explicit relation between ρ and $\boldsymbol{\sigma}$ makes it impossible to extend the connexion from U_{ij}^{*N} to $\boldsymbol{\sigma}$. This problem can be avoided by introducing U_{ij}^{*N} directly into $\dot{\boldsymbol{\epsilon}}$, this tensor being used itself for the computation of $\mathring{\boldsymbol{\sigma}}$ through (6). To achieve this, (30) is rewritten as:

$$\boldsymbol{\nabla}\boldsymbol{U}_i = \sum_{j\in\Omega_i} 2\left(\frac{\boldsymbol{U}_i + \boldsymbol{U}_j}{2} - \boldsymbol{U}_i\right) \otimes \boldsymbol{L}_i\boldsymbol{\nabla}W_{ij}V_j \tag{44}$$

Then, we use (38) to finally obtain:

$$\boldsymbol{\nabla}\boldsymbol{U}_i = \sum_{j\in\Omega_i} 2\left(\frac{\boldsymbol{U}_i + \boldsymbol{U}_j}{2} - \left(\frac{\boldsymbol{U}_i + \boldsymbol{U}_j}{2}\cdot\boldsymbol{n}_{ij}\right)\boldsymbol{n}_{ij} + U_{ij}^{*N}\boldsymbol{n}_{ij} - \boldsymbol{U}_i\right) \otimes \boldsymbol{L}_i\boldsymbol{\nabla}W_{ij}V_j \tag{45}$$

3) MUSCL applied to Parshikov and Medin's schemes: As formulated in [1], the left and right states for the Riemann problem are taken as $\phi_L = \phi_i$ and $\phi_R = \phi_j$, for any quantity ϕ. To increase the precision of the scheme, a linear reconstruction of the states at the interface can be applied to reach the first order approximation. Such a reconstruction is ensured by MUSCL [12] [9]. According to this scheme, ϕ_L and ϕ_R are now given by:

$$\phi_L = \phi_i + minmod(\boldsymbol{\nabla}^R\phi_i\cdot(\boldsymbol{x}_{ij} - \boldsymbol{x}_i), \phi_j - \phi_i) \tag{46}$$

$$\phi_R = \phi_j + minmod(\boldsymbol{\nabla}^R\phi_j\cdot(\boldsymbol{x}_{ij} - \boldsymbol{x}_j), \phi_i - \phi_j) \tag{47}$$

where $\boldsymbol{x}_{ij} = \frac{\boldsymbol{x}_i + \boldsymbol{x}_j}{2}$ and $minmod$ is a slope limiter defined by:

$$minmod(a,b) = max(0, min(a,b)) + min(0, max(a,b)) \tag{48}$$

The application of MUSCL for the Riemann-p scheme relies on the dependance between ρ and p. In this case, p and the components of $\boldsymbol{U}$ are reconstructed with MUSCL, then ρ is reconstructed from p via the reversed state equation. However, as mentionned before, there is no such relation between ρ and $\boldsymbol{\sigma}$. This lack of dependence between density

and stress tensor prevents us from applying MUSCL the same way in the context of the Riemann-$\boldsymbol{\sigma}$ scheme. This observation leads us to conduct two tests in the framework of the Riemann-$\boldsymbol{\sigma}$ scheme:

Test 1: This first naive test consists in extrapolating ρ, $\boldsymbol{U}$ and $\boldsymbol{\sigma}$ independently from one another,

Test 2: For this second test, MUSCL is only applied to $\boldsymbol{U}$ and to the diagonal components of $\boldsymbol{\sigma}$. Then, an intermediate pressure is calculated through (4) and used to obtain the extrapolated ρ through the inverse equation of state.

C. Boundary conditions

In this paper, boundary conditions are treated with the ghost particle method. As a reminder, this method consists in defining fictitious particles on the other side of the boundary in order to complete the partially filled kernel supports. For a particle i near the boundary, we need to define the quantities linked to a ghost particle g_i located in its kernel support. For the no-slip boundary condition, the velocity of g_i is given by:

$$\boldsymbol{u}_{g_i} = \boldsymbol{u}_i + 2[(\boldsymbol{u}_S - \boldsymbol{u}_i)\cdot \boldsymbol{n}_S]\boldsymbol{n}_S \tag{49}$$

where $\boldsymbol{u}_S$ and $\boldsymbol{n}_S$ are the boundary velocity and the normal at the boundary. If the momentum equation considered is (5), then the density (therefore the pressure) of g_i is obtained by applying the same method as the one used in [14] for fluid, but considering (13):

$$\rho_{g_i} = \rho_i \exp\left(-\frac{1}{c_o^2}\left[\left(\boldsymbol{f} - \frac{D\boldsymbol{u}_S}{Dt}\right)\cdot \boldsymbol{n}_S\right](\boldsymbol{x}_{g_i} - \boldsymbol{x}_i)\cdot \boldsymbol{n}_S\right) \tag{50}$$

and its deviatoric stress tensor is:

$$\boldsymbol{S}_{g_i} = \boldsymbol{S}_i \tag{51}$$

On the other hand, if the momentum equation considered is (2), then the stress tensor of g_i is [13]:

$$\boldsymbol{\sigma}_{g_i} = \boldsymbol{\sigma}_i \tag{52}$$

IV. Methods comparison

The performance of these methods are studied on two 2D benchmarks: the beam vibration and the impact of a wedge at the free-surface.

A. Beam vibration benchmark

First, the three schemes presented in the previous section are compared on the 2D beam vibration benchmark. The setup for this test is presented on figure 2. We consider an iron beam with the following characteristics:

$$L = 0.5\,m,\ h = 0.04\,m,\ \rho = 7800\,kg.m^{-3}$$
$$E = 200.10^9\,Pa,\ \nu = 0.3,\ c = 5064\,m.s^{-1}$$

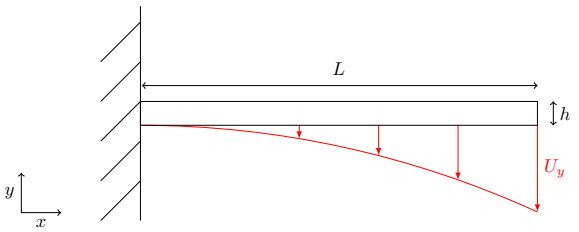

Fig. 2. Beam vibration case: Initial setup

The initial velocity U_y applied on the beam is given by:

$$U_y(x) = \xi\ c\ \frac{f(x)}{f(L)}$$

$$f(x) = (\cos kL + \cosh kL)(\cosh kx - \cos kx) + (\sin kL - \sinh kL)(\sinh kx - \sin kx)$$

where $\xi = -65.10^{-6}$ is an amplification factor for the velocity, and $k = 3.75$ rad.m^{-1} is the wave number. The deformation of the beam triggered by U_y is quantified by the deflection w. For practical reasons, results are given regarding the moment M about the z axis instead of w. These two quantities are linked by:

$$M = EI\frac{\partial^2 w}{\partial x^2} \tag{53}$$

where $I = 533.10^{-8}\,m^4$ is the quadratic moment of area of the beam. Since the δ-SPH scheme depends on two parameters, α and δ, we first study the influence of each of them separately in order to evaluate which values are the most adapted for this benchmark. First, we consider $\delta = 0.1$, according to [10].

Influence of α, with $\delta = 0.1$:
Figure 3(b) shows that with $\delta = 0.1$, the δ-SPH scheme is the least diffusive for α between 0.5 and 1. For these values, the phase shift between the theoretical moment and each of the simulated moments is the same. Besides, the stress field displayed on figure 3(a) are quite similar for these values, each of them presenting some Tensile Instability on the free edge of the beam. In the end, as a compromise between keeping diffusivity parameter rather low and getting satisfying simulation results, we choose to retain $\alpha = 0.5$ for the beam vibration simulation case.

Influence of δ, with $\alpha = 0.5$:
The achieved results with $\alpha = 0.5$ for different values of δ are really close: stress fields on figure 4(a) are all alike, and the simulated moments on figure 4(b) are practically overlapped, with a very similar phase shift and amplitude loss compared to the theoretical moment. Nevertheless, it appears that the scheme is the least diffusive with $\delta = 0.1$. Thus, we choose this parameter value for the simulations. To conclude, the couple $\alpha = 0.5$, $\delta = 0.1$ seems to be the most appropriate for this benchmark. The results for

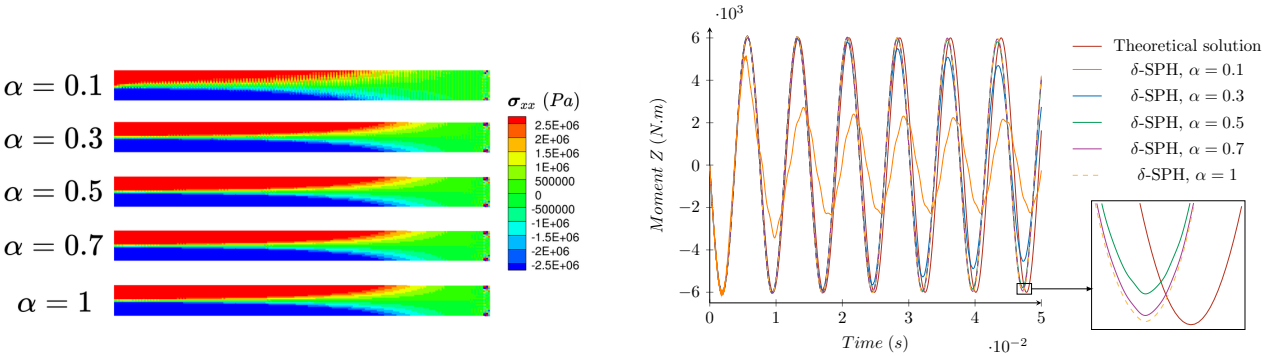

(a) Beam vibration case: Comparison of $\boldsymbol{\sigma}_{xx}$ at $t = 0.01\,s$

(b) Beam vibration case: Comparison of the moment

Fig. 3. Beam vibration case: Results depending on α

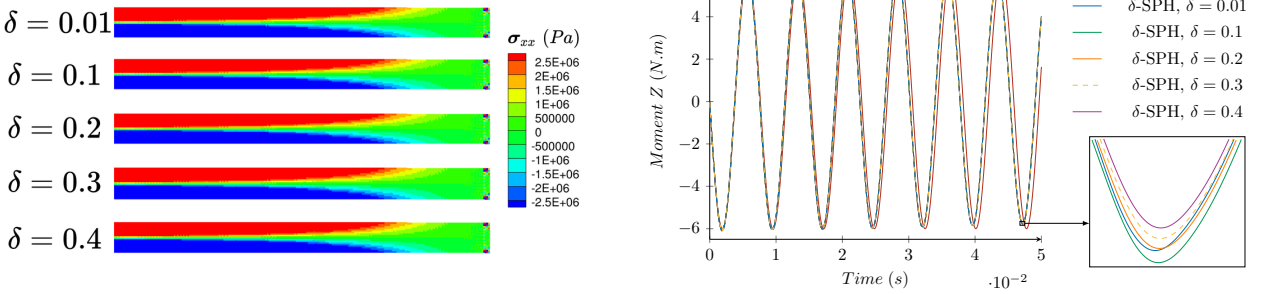

(a) Beam vibration case: Comparison of $\boldsymbol{\sigma}_{xx}$ at $t = 0.01\,s$

(b) Beam vibration case: Comparison of the moment

Fig. 4. Beam vibration case: Results depending on δ

δ-SPH can now be compared to those obtained with the two Riemann-SPH schemes introduced before.

Results comparison for the three methods:

Figure 5 and 6 show great similarity between the results achieved by δ-SPH and Riemann-p. The latter turns out to be the least diffusive scheme, but shares the same phase shift and problem of Tensile Instability at the end of the beam as δ-SPH.

Focusing now on Riemann-$\boldsymbol{\sigma}$, it appears that results differ significantly according to the method applied for MUSCL. First of all, test 1 seems to give convincing results, close to those obtained by the other methods. The stress field on figure 6 is even better with this scheme, as no Tensile Instability is observed with Riemann-$\boldsymbol{\sigma}$. However, the resulting moment of this first test, drawn in blue on figure 5, loses a little more amplitude over time than the two other methods. Consequently, Riemann-$\boldsymbol{\sigma}$ associated with the first application method for MUSCL is slightly more diffusive than Riemann-p and δ-SPH. By contrast, the second test on MUSCL is far less satisfying: while the stress field seems correct on the first time steps and does not display any signs of Tensile Instability either, the solution is however blatantly deteriorating over the simulation. A possible explanation for these results is the sensitivity of Riemann-$\boldsymbol{\sigma}$ to the MUSCL reconstruction, especially over the stress components. Indeed, different tests conducted with this scheme suggest that the reliability of Riemann-$\boldsymbol{\sigma}$ is greatly dependent on this reconstruction. Additional investigations are in progress to identify the source of this issue.

To conclude, the Riemann-$\boldsymbol{\sigma}$ scheme associated with the first MUSCL method gives conclusive results and, more importantly, provides a solution to cure the Tensile Instability problem in structures without adding diffusive terms in the equations as done by Gray et al [15].

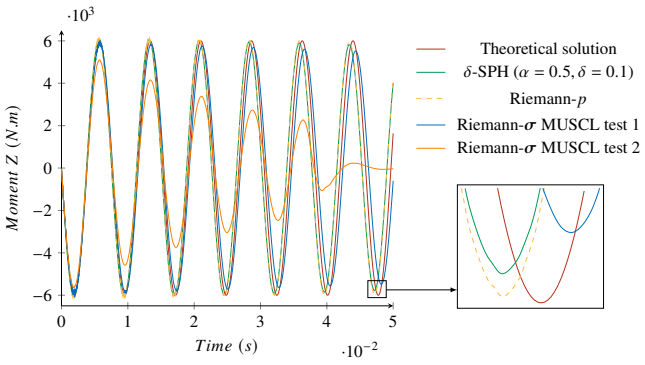

Fig. 5. Beam vibration case: Comparison of the moment

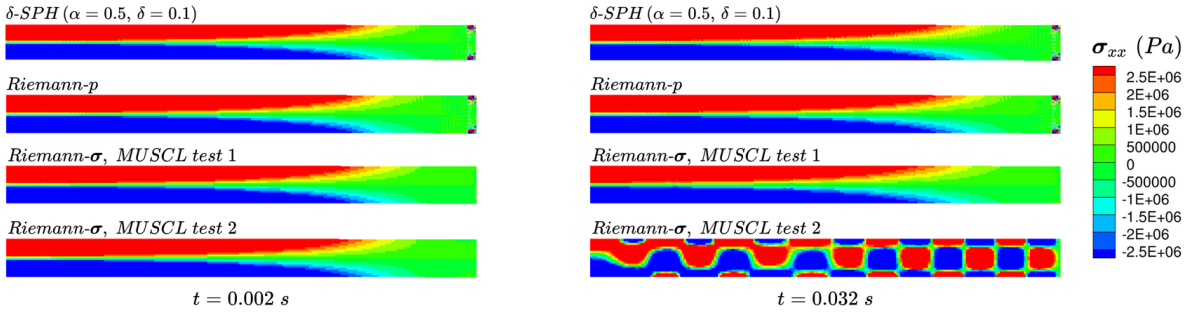

Fig. 6. Beam vibration case: Comparison of $\boldsymbol{\sigma}_{xx}$

B. Wedge impact benchmark

The second benchmark chosen to validate and compare the proposed methods is the 2D wedge impact, consisting of an inclined beam initially placed above water and impacting it with a high velocity. For this test, an aluminium beam with the following characteristics and clamped on both sides is considered, along with the setup described in figure 7:

$$L = 0.6\,m,\ h = 0.04\,m,\ \alpha = 10°,\ \rho = 2700\,kg.m^{-3}$$

$$E = 675.10^8\,Pa,\ \nu = 0.34,\ c = 5000\,m.s^{-1}$$

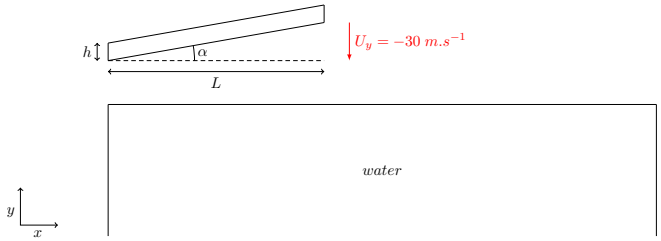

Fig. 7. Wedge impact case: Initial setup

Besides allowing to confirm the first observations made on the previous benchmark, this test-case offers the possibility to study how the fluid-structure interaction is handled by these methods. For δ-SPH, some problems concerning precisely this interaction emerged and could not be solved. Thus, only the two Riemann-SPH schemes are being tested here. Both of them were easily adapted to fluid-structure interaction, since the fluid is here supposed inviscid: concerning Riemann-p, the divergence term on $\boldsymbol{S}$ in (29) is removed when considering a fluid particle. For Riemann-$\boldsymbol{\sigma}$, the transition to the fluid is simply made by considering $\boldsymbol{\sigma} = -p\boldsymbol{I}$ and by changing the wave speeds (36) by:

$$c^l = c_0,\ c^t = 0 \tag{54}$$

The pressure calculated by both schemes on this benchmark are depicted on figure 8. They are very similar and consistent with the pressure profile provided in [16] for the same test-case. Nevertheless, when considering the deviatoric stress field on figure 9, the observations made earlier on the beam vibration benchmark are reiterated: while Tensile Instability is present on the left edge of the beam for Riemann-p, the solution obtained with Riemann-$\boldsymbol{\sigma}$ is perfectly smooth.

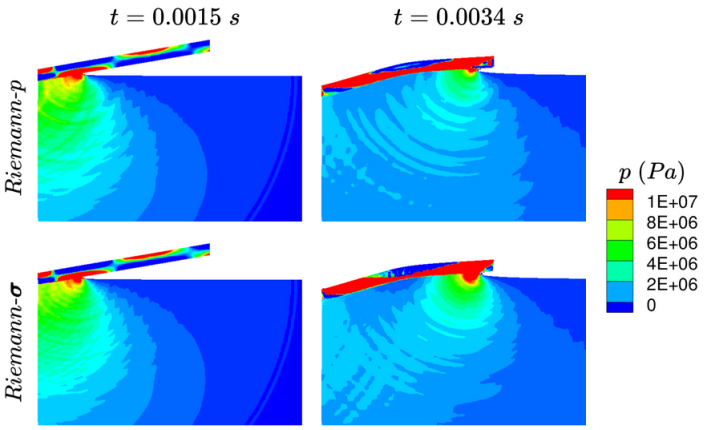

Fig. 8. Wedge impact case: Comparison of p

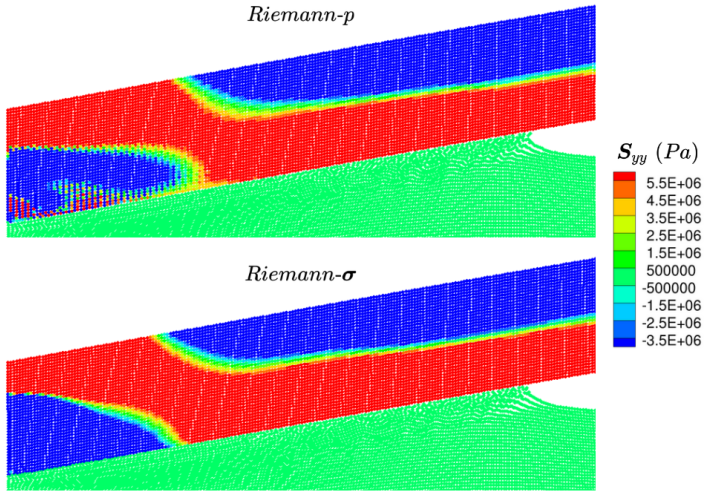

Fig. 9. Wedge impact case: Comparison of $\boldsymbol{S}_{yy}$ at $t = 0.0016\,s$

Further validations on this benchmark are in progress, using in particular Deuff's thesis results [16].

V. Conclusion

Two different stabilization methods are compared in the context of modelling elastic structures in SPH. On the one hand, a diffusive-term based stabilization is considered with the δ-SPH scheme adapted for structures. On the other hand, two schemes initially established by Parshikov and Medin [1] using a Riemann-based stabilization are presented and adapted for this problem. Both of them are then improved by applying MUSCL to increase their precision. The three resulting schemes give convincing results. In particular, the Riemann-$\boldsymbol{\sigma}$ scheme appears to avoid the Tensile Instability problem in structure while avoiding the need for tuning any diffusion parameter. However, as seen on figure 5, this scheme is more diffusive than the two others. Concerning δ-SPH, more optimal values may be found for the diffusion parameters α and δ, possibly offering a lower numerical diffusion.

Further investigations are planned in this direction, together with improvements on the Riemann-$\boldsymbol{\sigma}$ scheme, especially concerning the application of the MUSCL reconstruction. The impact of the scheme on the Tensile Instability problem will also be studied more precisely. Finally, its reliability will be tested on structures with more complex behaviours, in view of applying the model on granular flows.

Acknowledgment

The research leading to these results has received funding from the Région Pays de Loire R&D program 2020 through the "OSIRIS" project (Grant No. 2021-02676). This work was performed by using HPC resources of the Centrale Nantes Supercomputing Centre on the cluster Liger.

References

[1] A. N. Parshikov and S. A. Medin, *Smoothed particle hydrodynamics using interparticle contact algorithms*, J. Comp. Phys. 180: 358–382, 2002.

[2] R. Feng, G. Fourtakas, B.D. Rogers and D. Lombardi, *Modelling rainfall-induced slope collapse with Smoothed Particle Hydrodynamics (SPH)*, Proceedings of the 16th SPHERIC International Workshop, 268-275, 2022.

[3] H.H. Bui and G.D. Nguyen, *A coupled fluid-solid SPH approach to modelling flow through deformable porous media*, Int. J. Sol. Struc. 125: 244-264, 2017.

[4] A. Ghaïtanellis, *Modelling bed-load sediment transport through a granular approach in SPH*, PhD Thesis, Université Parie-Est, 2017.

[5] J. Von Neumann and R. D. Richtmyer, *A new method for the numerical calculation of hydrodynamics shocks*, J. App. Phys. 21: 232–247, 1950.

[6] J. J. Monaghan, *Smoothed particle hydrodynamics*, Annual Review of Astronomy and Astrophysics 30: 543–574, 1992.

[7] M. Antuono, A. Colagrossi, S. Marrone and D. Molteni, *Free-surface flows solved by means of SPH schemes with numerical diffusive terms*, Comp. Phys. Comm. 181(3): 532–549, 2010.

[8] S. Marrone, M. Antuono, A. Colagrossi, G. Colicchio, D. Le Touzé and G. Graziani, *δ-SPH model for simulating violent impact flows*, Comp. Meth. Appl. Mech. Eng. 200(13-16): 1526-1542, 2011.

[9] J.P. Vila, *On particle weighted methods and SPH*, Math. Mod. Meth. Appl. Sci., 9: 161–210, 1999.

[10] M. Antuono, A. Colagrossi and S. Marrone, *Numerical diffusive terms in weakly-compressible SPH schemes*, Comp. Phys. Comm. 183(12): 2570-2580, 2012.

[11] L.D. Landau and E.M. Lifshitz, *Theory of elasticity, Course of Theoretical Physics*, Volume VII, 1959.

[12] B. Van Leer, *Towards the ultimate conservative difference scheme. V. A second-order sequel to Godunov's method*, J. Comp. Phys. 32: 101–136, 1979.

[13] P.W. Randles and L.D. Libersky, *Smoothed particle hydrodynamics: some recent improvements and applications*, Comp. Meth. Appl. Mech. Eng. 139(1-4): 375, 1996.

[14] A. Vergnaud, *Améliorations de la précision et de la modélisation de la tension de surface au sein de la méthode SPH, et simulations de cas d'amerrissage d'urgence d'hélicoptères*, PhD Thesis, École Centrale de Nantes, 2020.

[15] J.P. Gray, J.J. Monaghan and R.P. Swift, *SPH elastic dynamics*, Comp. Meth. Appl. Mech. Eng. 190:6641-6662, 2001.

[16] J.B. Deuff, *Extrapolation au réel des mesures de pressions obtenues sur des cuves modèle réduit*, PhD Thesis, École Centrale de Nantes, 2007.